Deterministic three-photon down-conversion by a passive ultrastrong cavity-QED system

Kazuki Koshino[1,*] Tomohiro Shitara[1] Ziqiao Ao[2,3] and Kouichi Semba[3,†]
[1]*College of Liberal Arts and Sciences, Tokyo Medical and Dental University, Ichikawa, Chiba 272-0827, Japan*
[2]*Department of Advanced Science and Engineering, Waseda University, Tokyo 169-8555, Japan*
[3]*Advanced ICT Research Institute, National Institute of Information and Communications Technology, Koganei, Tokyo 184-8795, Japan*

(Received 6 September 2021; accepted 13 December 2021; published 6 January 2022)

In ultra- and deep-strong cavity quantum electrodynamics (QED) systems, many intriguing phenomena that do not conserve the excitation number are expected to occur. In this paper, we theoretically analyze the optical response of an ultrastrong cavity-QED system in which an atom is coupled to the first and third harmonic modes of a cavity, and report the possibility of deterministic three-photon down-conversion of itinerant photons upon reflection at the cavity. In the conventional parametric down-conversion, a strong input field is needed because of the smallness of the transition matrix elements of the higher-order processes. However, if we use an atom-cavity system in an unprecedentedly strong-coupling region, even a weak field in the linear-response regime is sufficient to cause this rare event involving the fourth-order transitions.

DOI: 10.1103/PhysRevResearch.4.013013

I. INTRODUCTION

The history of cavity quantum electrodynamics (QED) parallels with the enhancement of the atom-cavity coupling g. From the observations of the suppressed or enhanced atomic decay rate in the weak coupling regime ($g < \kappa, \gamma$, where κ and γ are the loss rates of the cavity and the atom, respectively) [1–5], more than a decade was required to reach the strong coupling regime ($g > \kappa, \gamma$), where the Rabi splitting or oscillation becomes observable [6–11]. Recently, the ultrastrong coupling regime ($g \gtrsim \omega_a/10, \omega_c/10$, where ω_a and ω_c are the resonance frequencies of the atom and cavity, respectively) and even the deep-strong coupling regime ($g \gtrsim \omega_a, \omega_c$) have been realized in various physical platforms such as polaritons, superconducting qubits, and molecules [12–18]. In the ultra- and deep-strong coupling regimes, various novel phenomena originating in the counter-rotating terms of the atom-cavity coupling are expected to become observable.

One of such phenomena is the deterministic nonlinear optics [19–23]. The generation efficiency of entangled photons, which is typically of the order of 10^{-6} for spontaneous parametric down-conversion with a bulk nonlinear crystal [24–26], might be drastically improved by this scheme. However, the proposed deterministic nonlinear-optical processes are for intracavity photons. In order to apply this scheme for itinerant photons, deterministic capturing of propagating photons into a cavity is indispensable. This is in principle possible but requires a precise dynamic control of the external cavity loss rate in accordance with the incoming photon shape [27,28]. In contrast, deterministic down-conversion of itinerant photons is possible and has been demonstrated in a passive waveguide QED setup [29–31]. The physical origin of the deterministic conversion is the destructive interference between incoming field and radiation from the atom. Accordingly, the efficiency is sensitive to the external loss rates of the relevant transitions of the atom.

In this paper, we investigate an ultrastrong cavity-QED system in which an atom is placed at the center of the cavity and is thus coupled to the first and third-harmonic modes of the cavity (Fig. 1) [32]. We show that, if the atom-cavity and cavity-waveguide couplings are adequately chosen, an input photon (resonant to the third mode) is down-converted nearly deterministically to three daughter photons (resonant to the first mode) upon reflection at the cavity. The drastic enhancement of the conversion efficiency in comparison with the prior demonstrations of triplet-photon generation [33–40] originates in the waveguide QED effect, in other words, the engineered dissipation rates of the optical system. Such deterministic conversion is possible even in the conventional strong-coupling cavity QED. However, considering the required intrinsic loss rates of the cavity modes, this phenomenon is characteristic to the ultrastrong cavity QED.

The rest of this paper is organized as follows. We present the theoretical model of the atom-cavity-waveguide coupled system in Sec. II. We observe the internal dynamics of the atom-cavity system and evaluate the effective coupling between the two levels relevant to three-photon down-conversion in Sec. III. We develop the input-output formalism applicable to the ultrastrong coupling regime in Sec. IV, and apply to the investigated setup in Sec. V. We numerically show that the deterministic three-photon down-conversion is possible in Sec. VI and clarify the required conditions. Section VII is devoted to a summary.

*kazuki.koshino@osamember.org
†Present address: Institute for Photon Science and Technology, The University of Tokyo, Tokyo 113-0033, Japan.

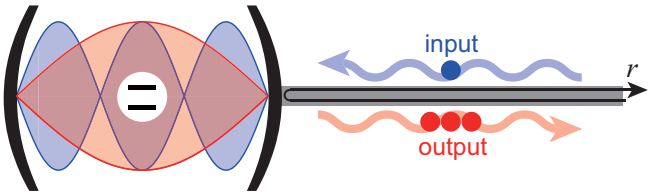

FIG. 1. Schematic of the considered setup. A qubit (resonance frequency ω_q) interacts with the first (ω_1) and third (ω_3) cavity modes with coupling constants g_1 and g_3, respectively. Dissipation channels are as follows: qubit radiative decay (rate γ), external and internal losses of the first cavity mode (κ_{1e}, κ_{1i}) and those for the third one (κ_{3e}, κ_{3i}). A weak monochromatic field (frequency $\omega_{\rm in} \sim \omega_3$) is input through the waveguide.

II. SYSTEM

In this paper, we investigate an optical response of a cavity-QED system schematically illustrated in Fig. 1. A two-level system (qubit) is placed at the center of a cavity and interacts with the first- and third-harmonic cavity modes. These cavity modes are coupled to an external waveguide field through the right mirror (capacitor, in circuit QED implementation), and a monochromatic field close to the resonance of the third cavity mode is applied through the waveguide.

The Hamiltonian of the qubit-cavity system is given, setting $\hbar = 1$, by

$$\hat{H}_s = \omega_q \hat{\sigma}^\dagger \hat{\sigma} + \omega_1 \hat{a}_1^\dagger \hat{a}_1 + \omega_3 \hat{a}_3^\dagger \hat{a}_3 + g_1 \hat{X}_1 \hat{X}_q + g_3 \hat{X}_3 \hat{X}_q, \quad (1)$$

where $\hat{\sigma}$, $\hat{a}_1$, and $\hat{a}_3$ respectively denote the annihilation operators of the qubit, the first and third cavity modes, and $\hat{X}_1 = \hat{a}_1^\dagger + \hat{a}_1$, $\hat{X}_3 = \hat{a}_3^\dagger + \hat{a}_3$, and $\hat{X}_q = \hat{\sigma}^\dagger + \hat{\sigma}$. ω_q, ω_1, and ω_3 denote their bare resonance frequencies, and g_1 and g_3 denote the qubit-cavity coupling strengths. Note that the counter-rotating terms are retained in order to treat the ultrastrong coupling regime.

We consider five dissipation channels of this system: the external/internal decay of the first/third cavity mode and the longitudinal decay of the qubit. We label these dissipation channels as $1e$, $1i$, $3e$, $3i$, and q, respectively, and denote their rates as κ_{1e}, κ_{1i}, κ_{3e}, κ_{3i}, and γ, respectively. As we observe later (Fig. 6), the investigated phenomenon is robust against the qubit dissipation, since the qubit excited state is used only virtually. We therefore neglect the qubit pure dephasing for simplicity, which plays essentially the same role as the longitudinal decay in the present phenomenon. The Hamiltonians describing the $1e$ and $3e$ channels are given by

$$\hat{H}_{1e} = \int_0^\infty dk \big[\omega_k \hat{c}_k^\dagger \hat{c}_k + \xi_k^{(1e)} \hat{X}_1 (\hat{c}_k^\dagger + \hat{c}_k)\big], \quad (2)$$

$$\hat{H}_{3e} = \int_0^\infty dk \big[\omega_k \hat{d}_k^\dagger \hat{d}_k + \xi_k^{(3e)} \hat{X}_3 (\hat{d}_k^\dagger + \hat{d}_k)\big], \quad (3)$$

where $\hat{c}_k$ ($\hat{d}_k$) is the annihilation operator of a waveguide mode with wavenumber k coupled to the first (third) cavity mode and ω_k is its frequency. The commutators for $\hat{c}_k$ and $\hat{d}_k$ are given by $[\hat{c}_k, \hat{c}_{k'}^\dagger] = [\hat{d}_k, \hat{d}_{k'}^\dagger] = \delta(k - k')$. Although these modes can be treated as a single continuum in principle, we may safely treat them as independent continua because of large separation between the relevant frequencies. The dispersion relation in the waveguide is linear, $\omega_k = k$, where the velocity of waveguide photons is set to unity for simplicity. A real quantity $\xi_k^{(je)}$ ($j = 1, 3$) represents the cavity-waveguide coupling. By naively applying the Fermi golden rule, the coupling and the decay rate are related by

$$\kappa_{je} = 2\pi \xi_{\omega_j}^{(je)2}. \quad (4)$$

The other loss channels are modeled similarly. For example, the longitudinal relaxation of the qubit is modeled by

$$\hat{H}_q = \int_0^\infty dk \big[\omega_k \hat{e}_k^\dagger \hat{e}_k + \xi_k^{(q)} \hat{X}_q (\hat{e}_k^\dagger + \hat{e}_k)\big]. \quad (5)$$

The relation to the qubit decay rate is $\gamma = 2\pi \xi_{\omega_q}^{(q)2}$.

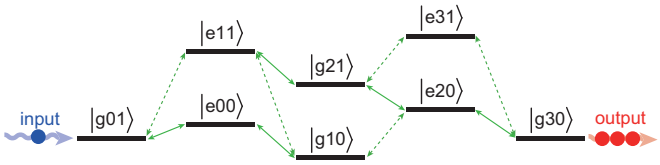

FIG. 2. Transition paths between $|g01\rangle$ and $|g30\rangle$. Solid (dotted) arrows indicate the transitions conserving (nonconserving) the excitation number.

III. COUPLING BETWEEN $|g01\rangle$ AND $|g30\rangle$

In this section, we investigate the properties of the qubit-cavity system, neglecting dissipation for the moment. We denote the state vector of the system by $|qmn\rangle$, where $q(= g, e)$ specifies the qubit state and m, n $(= 0, 1, \cdots)$ specify the photon numbers of the first and third cavity modes, respectively. In particular, we focus on the coupling between $|g01\rangle$ and $|g30\rangle$, which is essential for the three-photon down-conversion. Figure 2 shows the transition paths between $|g01\rangle$ and $|g30\rangle$. We observe that $|g01\rangle$ and $|g30\rangle$ are coupled through the fourth-order process in the qubit-cavity coupling $g_{1,3}$, and that transitions nonconserving the excitation number (dotted arrows in Fig. 2) are indispensable for their coupling.

For a strong coupling between these two states, degeneracy of these two states is required. The eigenenergies of $|g01\rangle$ and $|g30\rangle$ measured from $|g00\rangle$, which we denote by ε_{g01} and ε_{g30}, are renormalized by the dispersive qubit-cavity coupling and depend on $g_{1,3}$ and ω_q. In Fig. 3(a), by numerically diagonalizing $\hat{H}_s$ [taking into account up to the 6 (2) photon states for $\hat{a}_1$ ($\hat{a}_3$) mode], ε_{g01} and ε_{g30} are plotted as functions of the qubit frequency ω_q. We observe an anticrossing between them, and from this plot we can identify the following quantities. (i) The optimal qubit frequency $\omega_q^{\rm opt}$, at which the level spacing is minimized. (ii) The effective coupling $g_{\rm eff}$ between $|g01\rangle$ and $|g30\rangle$, which is half of the level spacing at $\omega_q^{\rm opt}$. (iii) The optimal input photon frequency $\omega_{\rm in}^{\rm opt}$, which is the average of the two transition frequencies at $\omega_q^{\rm opt}$. In Figs. 3(b) and 3(c), assuming $3\omega_1 = \omega_3 = 2\pi \times 9\,{\rm GHz}$ and $g_1 = g_3 (= g)$, we plot $\omega_q^{\rm opt}$, $\omega_{\rm in}^{\rm opt}$ and $g_{\rm eff}$ as functions of g.

We can confirm in Fig. 3(c) that $g_{\rm eff}$ is proportional to g^4, which is consistent with the fact that $|g01\rangle$ and $|g30\rangle$ are coupled through the fourth-order process. The analytic expression of $g_{\rm eff}$ is derived perturbatively in Appendix A.

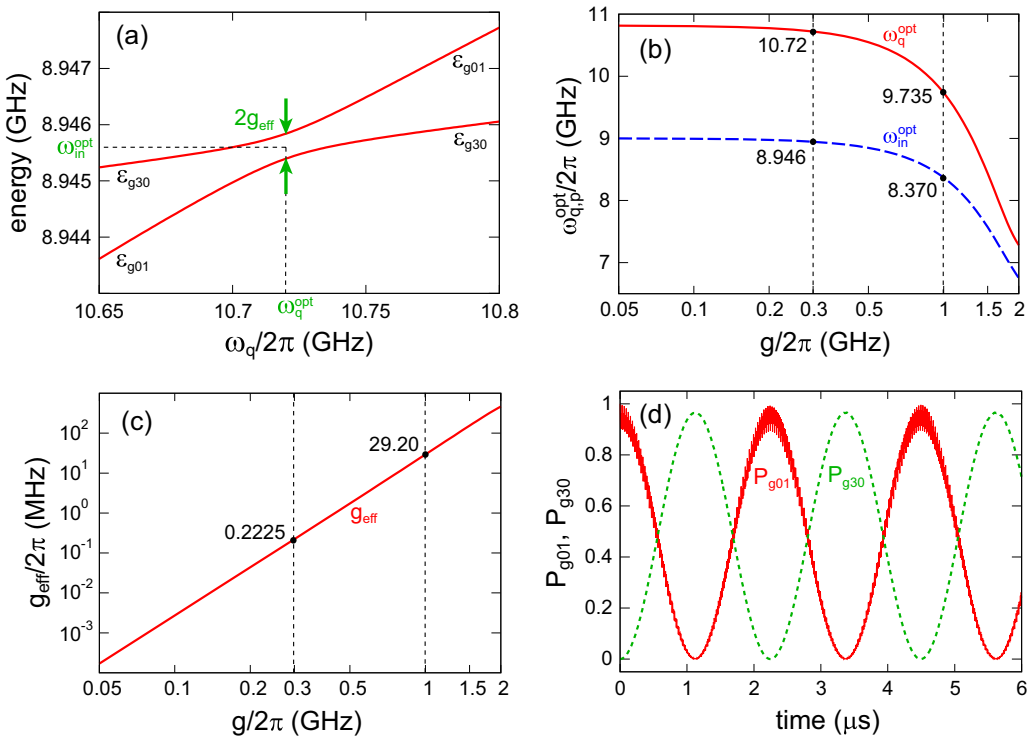

FIG. 3. Effective coupling between $|g01\rangle$ and $|g30\rangle$. $3\omega_1 = \omega_3 = 2\pi \times 9$ GHz and $g_1 = g_3 (= g)$ are assumed. (a) Anticrossing between $|g01\rangle$ and $|g30\rangle$ varying the qubit frequency ω_q. $g = 2\pi \times 0.3$ GHz. [(b), (c)] Dependences of $\omega_q^{\rm opt}$, $\omega_{\rm in}^{\rm opt}$, and $g_{\rm eff}$ on the qubit-cavity coupling g. Specific values at $g = 2\pi \times 0.3$ and 1 GHz are indicated. (d) Vacuum Rabi oscillation between $|g01\rangle$ and $|g30\rangle$, starting from $|g01\rangle$. $g = 2\pi \times 0.3$ GHz and $\omega_q = \omega_q^{\rm opt} = 2\pi \times 10.72$ GHz.

We also observe in Fig. 3(b) that, in the weak-coupling limit of $g \to 0$, $\omega_{\rm in}^{\rm opt} \to \omega_3 = 3\omega_1 = 2\pi \times 9$ GHz and $\omega_q^{\rm opt} \to \sqrt{(3\omega_3^2 - \omega_1^2)/2} = 2\pi \times 10.82$ GHz. This optimal qubit frequency in the weak-coupling limit is derived as follows. Within the second-order perturbation in g_1 and g_3, ε_{g01} and ε_{g30} are renormalized as $\varepsilon_{g01} = \omega_3 - \frac{g_3^2}{\omega_q - \omega_3} - \frac{g_3^2}{\omega_q + \omega_3}$ and $\varepsilon_{g30} = 3(\omega_1 - \frac{g_1^2}{\omega_q - \omega_1} - \frac{g_1^2}{\omega_q + \omega_1})$, respectively. The degeneracy condition, $\varepsilon_{g01} = \varepsilon_{g30}$, reduces to $\omega_q = \sqrt{(3\omega_3^2 - \omega_1^2)/2}$ for the present case of $\omega_3 = 3\omega_1$ and $g_1 = g_3$.

In Fig. 3(d), coherent time evolution of the system starting from $|g01\rangle$ is shown. We observe the vacuum Rabi oscillation between $|g01\rangle$ and $|g30\rangle$. The oscillation is not pure sinusoidal, since other states than $|g01\rangle$ and $|g30\rangle$ (such as $|e00\rangle$) are involved in forming the eigenstates. The Rabi oscillation period measured in Fig. 3(d) is $T = 2.247$ μs. This is compatible with $g_{\rm eff} = 2\pi \times 222.5$ kHz evaluated from Fig. 3(a), because $g_{\rm eff} T/\pi \approx 1$.

IV. INPUT-OUTPUT FORMALISM FOR ULTRASTRONG CAVITY QED

In the following part of this paper, we analyze the response of the qubit-cavity system to a waveguide field. For this purpose, the input-output formalism is useful. However, although highly useful in the weak- and (usual) strong-coupling regimes of cavity QED, the conventional formalism based on the white reservoir approximation has several difficulties in treating the ultrastrong cavity QED [17]. The input-output formalism applicable to the ultrastrong cavity QED has been discussed first in linear systems [41] and later extended to nonlinear systems [42,43]. However, assuming weak dissipation, the counter-rotating terms in the system-environment coupling have been neglected in prior works. In this section, in order to extend the formalism applicable to highly dissipative cases, we develop an input-output formalism incorporating the counter-rotating terms in the system-environment coupling.

A. Heisenberg equations

In this section, for simplicity, we consider a case in which the cavity-QED system is coupled only to the $1e$ dissipation channel. Namely, the overall Hamiltonian is given by $\hat{H} = \hat{H}_s + \hat{H}_{1e}$. We also introduce the following abbreviations throughout this section: $\xi_k^{(1e)} \to \xi_k$ and $\hat{X}_1 \to \hat{X}$.

The Heisenberg equation of $\hat{c}_k$ is given by $d\hat{c}_k/dt = i[\hat{H}, \hat{c}_k] = -ik\hat{c}_k - i\xi_k \hat{X}$, which is formally integrated as

$$\hat{c}_k(t) = \hat{c}_k(0) e^{-ikt} - i\xi_k \int_0^t d\tau\, e^{-ik\tau} \hat{X}(t-\tau). \tag{6}$$

The Heisenberg equation of an arbitrary system operator $\hat{S}$ is given by $d\hat{S}/dt = i[\hat{H}_s, \hat{S}] + i\int_0^\infty dk\, \xi_k [\hat{X}, \hat{S}](\hat{c}_k^\dagger + \hat{c}_k)$. Using Eq. (6), this becomes a delay differential equation,

$$\frac{d}{dt}\hat{S} = i[\hat{H}_s, \hat{S}] + \int_0^\infty dk \int_0^t d\tau\, \xi_k^2 (e^{-ik\tau}[\hat{X}, \hat{S}]\hat{X}(t-\tau) - e^{ik\tau}\hat{X}(t-\tau)[\hat{X}, \hat{S}]) + i[\hat{X}, \hat{S}]\hat{\Gamma}(t) + i\hat{\Gamma}^\dagger(t)[\hat{X}, \hat{S}], \tag{7}$$

where $\hat{\Gamma}(t)$ is a noise operator defined by

$$\hat{\Gamma}(t) = \int_0^\infty dk\ \xi_k e^{-ikt}\hat{c}_k(0). \tag{8}$$

In Eq. (7) and hereafter, we omit explicit time-dependence for the operators at time t in the Heisenberg picture. Note that the noise operator $\hat{\Gamma}(t)$ is *not* in the Heisenberg picture.

In order to convert a delay differential equation (7) into an instantaneous one, we employ a *free-evolution* approximation for the time evolution of the system operator during the delay time τ [44–46]. We denote the eigenstates and eigenenergies of $\hat{H}_s$ by $|j\rangle$ and ε_j $(j = 0, 1, \cdots)$ in the energy-increasing order, and define the transition operator by $\hat{s}_{ij} = |i\rangle\langle j|$. We then approximate $\hat{X}(t-\tau)$ as

$$\hat{X}(t-\tau) = \sum_{i,j} x_{ij}\hat{s}_{ij}(t-\tau) \approx \sum_{i,j} x_{ij}e^{i\varepsilon_{ji}\tau}\hat{s}_{ij}(t), \tag{9}$$

where $x_{ij} = \langle i|\hat{X}|j\rangle$ and $\varepsilon_{ji} = \varepsilon_j - \varepsilon_i$. In this approximation, we assume free time evolution of the system operators during the delay time, neglecting the higher-order system-waveguide interactions that are implicitly included in $\hat{X}(t-\tau)$. This is essentially the same as the Markov approximation in the derivation of master equation in the interaction picture. Then, Eq. (7) is rewritten as

$$\begin{aligned}\frac{d}{dt}\hat{S} = {} & i[\hat{H}_s, \hat{S}] + [\hat{X}, \hat{S}]\hat{A} - \hat{A}^\dagger[\hat{X}, \hat{S}] \\ & + i[\hat{X}, \hat{S}]\hat{\Gamma}(t) + i\hat{\Gamma}^\dagger(t)[\hat{X}, \hat{S}],\end{aligned} \tag{10}$$

where

$$\hat{A} = \sum_{i,j} x_{ij}h_{ji}\hat{s}_{ij}, \tag{11}$$

and $h_{ji} = \int_0^t d\tau \int_0^\infty dk\ \ \xi_k^2 e^{i(\varepsilon_{ji}-k)\tau}$. Strictly speaking, this quantity depends on t. However, since $\int_0^\infty dk\ \xi_k^2 e^{-ik\tau}$ is nonzero only for short τ ($\sim$ inversed bandwidth of ξ_k^2), we can safely treat h_{ji} as a t-independent quantity, $h_{ji} \approx \int_0^\infty d\tau \int_0^\infty dk\ \xi_k^2 e^{i(\varepsilon_{ji}-k)\tau}$. Then we have

$$\begin{aligned}h_{ji} &= -i\int_0^\infty dk \frac{\xi_k^2}{k - \varepsilon_{ji} - i0} \\ &= \pi\theta(\varepsilon_{ji})\xi_{\varepsilon_{ji}}^2 - i\mathrm{P}\int_0^\infty dk \frac{\xi_k^2}{k-\varepsilon_{ji}},\end{aligned} \tag{12}$$

where θ is the Heaviside step function and P represents the principal value. This is a self-energy correction to the transition frequency: the real part corresponds to half of the decay rate and the imaginary part corresponds the Lamb shift [47]. Note that the real part vanishes for negative ε_{ji}, reflecting the prohibited decay from a lower level to an upper level.

B. Waveguide-field operator

For a semi-infinite waveguide (Fig. 1), the waveguide eigenmodes are the standing wave extending in the $r > 0$ region. Assuming an open boundary condition at $r = 0$, the eigenmode function f_k with wavenumber k is given by $f_k(r) = \sqrt{2/\pi}\cos(kr)\theta(r)$, which is orthonormalized as $\int_0^\infty dr f_k(r)f_{k'}(r) = \delta(k-k')$. Accordingly, the waveguide mode operator $\hat{c}_r$ in the real-space representation is defined in the $r > 0$ region by $\hat{c}_r(t) = \sqrt{2/\pi}\int_0^\infty dk\cos(kr)\hat{c}_k(t)$, which satisfies the commutation relation $[\hat{c}_r, \hat{c}_{r'}^\dagger] = \delta(r-r')$. The incoming field propagates in the $r > 0$ region into the negative direction ($k < 0$).

However, it is convenient to treat the incoming field as if it propagates in the $r < 0$ region into the positive direction ($k > 0$). We therefore introduce the real-space representation by

$$\widetilde{c}_r(t) = \frac{1}{\sqrt{2\pi}}\int_0^\infty dk\ e^{ikr}\hat{c}_k(t), \tag{13}$$

where r runs over the full one-dimensional space ($-\infty < r < \infty$) [48]. From Eq. (6), we have

$$\widetilde{c}_r(t) = \widetilde{c}_{r-t}(0) - \frac{i}{\sqrt{2\pi}}\int_0^\infty dk \int_0^t d\tau\ \xi_k e^{ik(r-\tau)}\hat{X}(t-\tau). \tag{14}$$

This equation represents the waveguide-field operator in terms of the input-field operator and the system operator, and enables, for example, evaluation of the output-field amplitude and flux.

C. Input-output relation

We can further simplify Eq. (14) under some approximations. Introducing $\tau' = \tau - r$ and employing the free-evolution approximation, $\hat{X}(t-r-\tau') = \sum_{i,j} x_{ij}\hat{s}_{ij}(t-r)e^{i\omega_{ij}\tau'}$, Eq. (14) is rewritten as

$$\widetilde{c}_r(t) = \widetilde{c}_{r-t}(0) + \sum_{i,j} x_{ij}f(\varepsilon_{ji}, r, t)\hat{s}_{ij}(t-r), \tag{15}$$

$$f(\varepsilon, r, t) = \frac{1}{\sqrt{2\pi}}\int_0^\infty dk \frac{\xi_k}{k-\varepsilon}[e^{i(k-\varepsilon)(r-t)} - e^{i(k-\varepsilon)r}]. \tag{16}$$

Note that the integrand in the right-hand side of Eq. (16) is not singular at $k = \varepsilon$. We can approximately evaluate $f(\varepsilon, r, t)$ as follows. Since the main contribution of this integral comes from the $k \approx \varepsilon$ region, we set $\xi_k \approx \xi_\varepsilon\theta(\varepsilon)$ and remove the lower limit of k integral as $\int_0^\infty \approx \int_{-\infty}^\infty$. Then we have

$$f_{\mathrm{app}}(\varepsilon, r, t) = -i\sqrt{2\pi}\xi_\varepsilon\theta(\varepsilon)\theta(r)\theta(t-r). \tag{17}$$

In Appendix B, we observe fairly good agreement between $f(\varepsilon, r, t)$ and $f_{\mathrm{app}}(\varepsilon, r, t)$, assuming a concrete form of ξ_k [Eq. (28)]. Thus we have

$$\widetilde{c}_r(t) = \widetilde{c}_{r-t}(0) - i\sqrt{2\pi}\theta(r)\theta(t-r)\sum_{i<j}\xi_{\varepsilon_{ji}}x_{ij}\hat{s}_{ij}(t-r). \tag{18}$$

Note that the summation over i and j is conditioned by $i < j$ in Eq. (18), which is due to the following reasons. (i) For $i > j$, ε_{ji} is negative and accordingly $\theta(\varepsilon_{ji}) = 0$. (ii) For $i = j$, $x_{ij} = 0$ due to the parity selection rule. Defining the input and output field operators by $\hat{c}_{\mathrm{in}}(t) = \widetilde{c}_{-0}(t) = \widetilde{c}_{-t}(0)$ and $\hat{c}_{\mathrm{out}}(t) = \widetilde{c}_{+0}(t)$, Eq. (18) is rewritten into a more familiar form,

$$\hat{c}_{\mathrm{out}}(t) = \hat{c}_{\mathrm{in}}(t) - i\sqrt{2\pi}\sum_{i<j}\xi_{\varepsilon_{ji}}x_{ij}\hat{s}_{ij}(t). \tag{19}$$

V. OPTICAL RESPONSE THEORY

A. Initial state vector

In this paper, instead of a single photon pulse, we apply a weak classical monochromatic field close to the resonance of the third cavity mode [$\mathcal{E}_{\rm in}(t) = E_{\rm in}e^{-i\omega_{\rm in}t}$ with $\omega_{\rm in} \sim \omega_3$] to the cavity (Fig. 1). Assuming that, at the initial moment ($t = 0$), the overall system is in the vacuum state except the applied field, the initial state vector is written as

$$|\psi_i\rangle = \exp\left(\sqrt{2\pi}E_{\rm in}\hat{d}^\dagger_{\omega_{\rm in}} - \sqrt{2\pi}E^*_{\rm in}\hat{d}_{\omega_{\rm in}}\right)|vac\rangle, \quad (20)$$

where $|vac\rangle$ is the overall vacuum state. Note that this is an eigenstate of the noise operators: $\hat{\Gamma}^{(3e)}(t)|\psi_i\rangle = \sqrt{2\pi}\xi^{(3e)}_{\omega_{\rm in}}\mathcal{E}_{\rm in}(t)|\psi_i\rangle$ and $\hat{\Gamma}^{(j)}(t)|\psi_i\rangle = 0$ for $j = 1e, 1i, 3i$, and q.

B. Density matrix elements

The Heisenberg equation for a system operator is given by Eq. (10) with the dissipators and the noise operators corresponding to the five decay channels ($1e$, $1i$, $3e$, $3i$, and q). The equation of motion for $s_{ij}(t) = \langle\psi_i|\hat{s}_{ij}(t)|\psi_i\rangle$, which is identical to the density matrix element $\rho_{ji}(t) = \langle j|\hat{\rho}(t)|i\rangle$ in the Schrödinger picture, is then given by

$$\frac{d}{dt}s_{ij} = \sum_{m,n}\eta^{(a)}_{ijmn}s_{mn} + \mathcal{E}^*_{\rm in}(t)\sum_{m,n}\eta^{(b)}_{ijmn}s_{mn} + \mathcal{E}_{\rm in}(t)\sum_{m,n}\eta^{(c)}_{ijmn}s_{mn}, \quad (21)$$

where the coefficients $\eta^{(a,b,c)}_{ijmn}$ are given by

$$\begin{aligned}\eta^{(a)}_{ijmn} &= i(\varepsilon_i - \varepsilon_j)\delta_{im}\delta_{jn} + x^{(1)}_{mi}x^{(1)}_{jn}\left(h^{(1)}_{nj} + h^{(1)*}_{mi}\right) - \delta_{im}\left(\sum_l x^{(1)}_{jl}x^{(1)}_{ln}h^{(1)}_{nl}\right) - \delta_{jn}\left(\sum_l x^{(1)}_{il}x^{(1)}_{lm}h^{(1)*}_{ml}\right)\\ &+ x^{(3)}_{mi}x^{(3)}_{jn}\left(h^{(3)}_{nj} + h^{(3)*}_{mi}\right) - \delta_{im}\left(\sum_l x^{(3)}_{jl}x^{(3)}_{ln}h^{(3)}_{nl}\right) - \delta_{jn}\left(\sum_l x^{(3)}_{il}x^{(3)}_{lm}h^{(3)*}_{ml}\right)\\ &+ x^{(q)}_{mi}x^{(q)}_{jn}\left(h^{(q)}_{nj} + h^{(q)*}_{mi}\right) - \delta_{im}\left(\sum_l x^{(q)}_{jl}x^{(q)}_{ln}h^{(q)}_{nl}\right) - \delta_{jn}\left(\sum_l x^{(q)}_{il}x^{(q)}_{lm}h^{(q)*}_{ml}\right), \quad (22)\end{aligned}$$

$$\eta^{(b)}_{ijmn} = i\sqrt{2\pi}\xi^{(3e)}_{\omega_d}\left(x^{(3)}_{mi}\delta_{jn} - x^{(3)}_{jn}\delta_{im}\right), \quad (23)$$

$$\eta^{(c)}_{ijmn} = \left(\eta^{(2)}_{ijmn}\right)^*, \quad (24)$$

where $x^{(s)}_{mn} = \langle m|\hat{X}_s|n\rangle$ for $s = 1, 3, q$, and $h^{(s)}_{mn} = h^{(se)}_{mn} + h^{(si)}_{mn}$ for $s = 1, 3$. In this paper, we apply a continuous field and observe the stationary response of the system. Therefore, we numerically determine the stationary solution of these simultaneous equations by perturbation with respect to $\mathcal{E}_{\rm in}(t)$. Further details on analysis are presented in Appendix C.

C. Photon flux

Since we treat a stationary input/output field, we quantify the amount of photons by the photon flux, namely, the rate of incoming/outgoing photons per unit time. The input photon flux is evaluated by $F_{\rm in} = \langle\psi_i|\hat{d}^\dagger_{\rm in}(t)\hat{d}_{\rm in}(t)|\psi_i\rangle$. From Eq. (20), this quantity reduces to

$$F_{\rm in} = |\mathcal{E}_{\rm in}(t)|^2 = |E_{\rm in}|^2. \quad (25)$$

In the output port, the fluxes of down-converted and unconverted photons are respectively evaluated by $F^1_{\rm out} = \langle\psi_i|\hat{c}^\dagger_{\rm out}(t)\hat{c}_{\rm out}(t)|\psi_i\rangle$ and $F^3_{\rm out} = \langle\psi_i|\hat{d}^\dagger_{\rm out}(t)\hat{d}_{\rm out}(t)|\psi_i\rangle$. From Eq. (19) and its counterpart for $\hat{d}_{\rm out}$, these quantities are given by

$$F^1_{\rm out} = 2\pi\sum_{i,j}\left(\sum_m x^{(1)}_{mi}x^{(1)}_{mj}\xi^{(1e)}_{\varepsilon_{im}}\xi^{(1e)}_{\varepsilon_{jm}}\right)s_{ij}(t), \quad (26)$$

$$\begin{aligned}F^3_{\rm out} &= |\mathcal{E}_{\rm in}(t)|^2 + 2\pi\sum_{i,j}\left(\sum_m x^{(3)}_{mi}x^{(3)}_{mj}\xi^{(3e)}_{\varepsilon_{im}}\xi^{(3e)}_{\varepsilon_{jm}}\right)s_{ij}(t)\\ &+ i\sqrt{2\pi}\sum_{i,j}\xi^{(3e)}_{\varepsilon_{ji}}x^{(3)}_{ij}[s_{ji}(t)\mathcal{E}_{\rm in}(t) - \text{c.c.}]. \quad (27)\end{aligned}$$

VI. NUMERICAL RESULTS

In this section, we present the numerical results on the optical response, fixing the bare cavity frequencies at $3\omega_1 = \omega_3 = 2\pi \times 9\,$GHz. For reduction of parameters, we restrict ourselves to the case of $g_1 = g_3$, $\kappa_{1e} = \kappa_{3e}$ and $\kappa_{1i} = \kappa_{3i}$ and denote them by g, κ_e, and κ_i, respectively. Furthermore, regarding the coupling for the $1e$ decay channel for example, we assume the following form:

$$\xi^{(1e)}_k = \theta(k)\theta(k_x - k)\sqrt{\kappa_{1e}/2\pi}, \quad (28)$$

where k_x is the cutoff wavenumber. Note that this coupling satisfies Eq. (4). We fix k_x at $2\pi \times 20\,$GHz and confirmed that numerical results are mostly insensitive to k_x. The other system-environment couplings are defined similarly and with the same cutoff wavenumber. From Eq. (12), $h^{(1e)}_{ji}$ is analytically given by

$$h^{(1e)}_{ji} = \frac{\kappa_{1e}}{2}\theta(\varepsilon_{ji})\theta(k_x - \varepsilon_{ji}) - \frac{i\kappa_{1e}}{2\pi}\log\left(\frac{|k_x - \varepsilon_{ji}|}{|\varepsilon_{ji}|}\right). \quad (29)$$

Regarding the input field power, we assume the weak-field limit in Secs. VI A–VI C, and discuss the input power dependence in Sec. VI D.

A. Optimal condition for κ_e

First, we search the optimal value of κ_e assuming no intrinsic losses ($\kappa_i = \gamma = 0$). Figures 4(a) and 4(b) show the dependence of the down-converted flux $F^1_{\rm out}$ on κ_e and $\omega_{\rm in}$, fixing g and ω_q. It is observed that $F^1_{\rm out}$ has two peaks for small

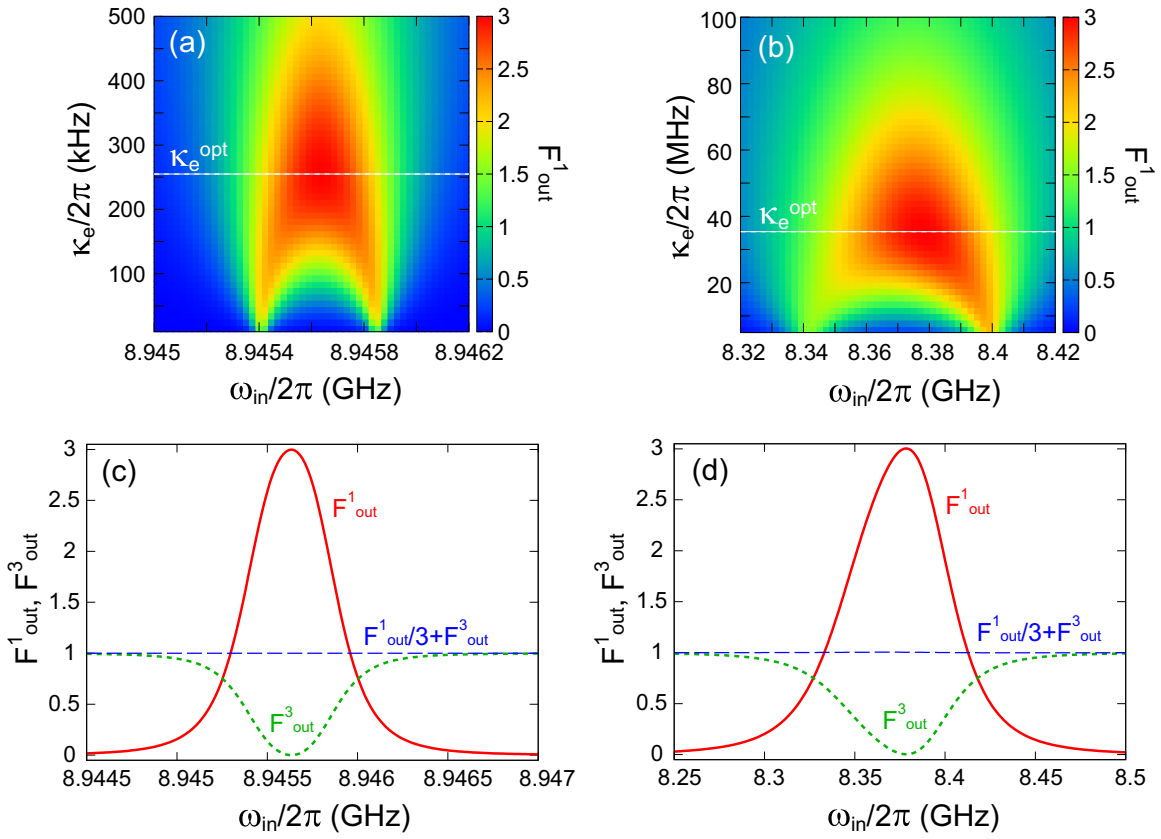

FIG. 4. Optimization of κ_e assuming no intrinsic losses ($\kappa_i = \gamma = 0$). The output photon fluxes, $F^{1,3}_{out}$, are normalized by the input flux, F_{in}. (a) Dependence of the down-converted flux F^1_{out} on κ_e and ω_{in}, for $(g, \omega_q) = 2\pi \times (0.3, 10.72)$ GHz. The optimal point is $(\kappa_e^{opt}, \omega_{in}^{opt}) = 2\pi \times (255.0\,\text{kHz}, 8.9456\,\text{GHz})$. (b) Same plot as (a) for $(g, \omega_q) = 2\pi \times (1.0, 9.735)$ GHz. The optimal point is $(\kappa_e^{opt}, \omega_{in}^{opt}) = 2\pi \times (35.4\,\text{MHz}, 8.378\,\text{GHz})$. (c) Cross section of (a) at κ_e^{opt}: down-converted flux F^1_{out} (solid), unconverted flux F^3_{out} (dotted), and $F^1_{out}/3 + F^3_{out}$ (thin dashed). (d) Cross section of (b) at κ_e^{opt}.

κ_e. This is due to the Rabi splitting of $|g30\rangle$ and $|g01\rangle$, and the frequency difference of the two peaks agrees with $2g_{eff}$ in Fig. 3(c). F^1_{out} is maximized for a larger κ_e, at which the two peaks become spectrally indistinguishable. Therefore, the optimal condition for the external loss rate of the cavity is given by $\kappa_e^{opt} \sim g_{eff}$. We confirm in Appendix D that this condition is identical to the impedance-matching condition of a linear optical system composed of oscillators and waveguides. Actually, we can confirm in Figs. 4(a) and 4(b) that κ_e^{opt} is $2\pi \times 255$ kHz (35.4 MHz) for $g = 2\pi \times 0.3$ GHz (1.0 GHz). This is almost identical to $g_{eff} = 2\pi \times 223$ kHz (29.2 MHz) in Fig. 3(c).

Figures 4(c) and 4(d) are the cross section of Figs. 4(a) and 4(b) at κ_e^{opt}. It is observed that the deterministic down-conversion ($F^1_{out} \approx 3F_{in}$ and $F^3_{out} \approx 0$) is attained regardless of the value of g, when the input photon frequency ω_{in} is optimally chosen. Furthermore, reflecting the absence of intrinsic loss channels, we can also confirm the energy conservation, $F^1_{out}/3 + F^3_{out} \approx F_{in}$, for any input photon frequency. However, by carefully examining the numerical results, this conservation law is slightly broken at the order of 10^{-5} [10^{-3}] in Fig. 4(c) [Fig. 4(d)]. We attribute the main reason for this slight discrepancy to the free-evolution approximation [Eq. (9)], whose validity is gradually lost for larger dissipation rates.

B. Qubit detuning

Here, assuming again the absence of intrinsic losses, we observe the effects of the qubit detuning from its optimal value. Figure 5 shows the dependence of the down-converted flux F^1_{out} on ω_q and ω_{in}, fixing κ_e at its optimal value [255 kHz in (a) and 35.4 MHz in (b)]. It is observed that, as the qubit-cavity coupling g increases, the deterministic down-conversion becomes more robust against the qubit detuning. This is because of the increase of the optimal qubit linewidth for larger g. The allowed qubit detuning (the full width in ω_q at the half maximum of the cross-sectional plot at the optimal ω_{in}) is about 20 MHz (240 MHz) for $g = 2\pi \times 0.3$ GHz (1.0 GHz).

C. Intrinsic losses

Here, we investigate the effects of intrinsic losses of the qubit and cavity. Figures 6(a) and 6(b) show the dependence of the down-converted flux F^1_{out} on γ and κ_i, fixing the other parameters at their optimal values. When $g = 2\pi \times 0.3$ GHz, the deterministic down-conversion is highly vulnerable to the intrinsic losses. The condition for achieving 50% conversion ($F^1_{out} > 1.5$) is $\kappa_i \lesssim 2\pi \times 92.9$ kHz (intrinsic quality factor $Q_i \gtrsim 3.23 \times 10^4$ for the first cavity mode) and $\gamma \lesssim 2\pi \times 5.55$ MHz (lifetime $T_1 \gtrsim 28.7$ ns). These conditions are

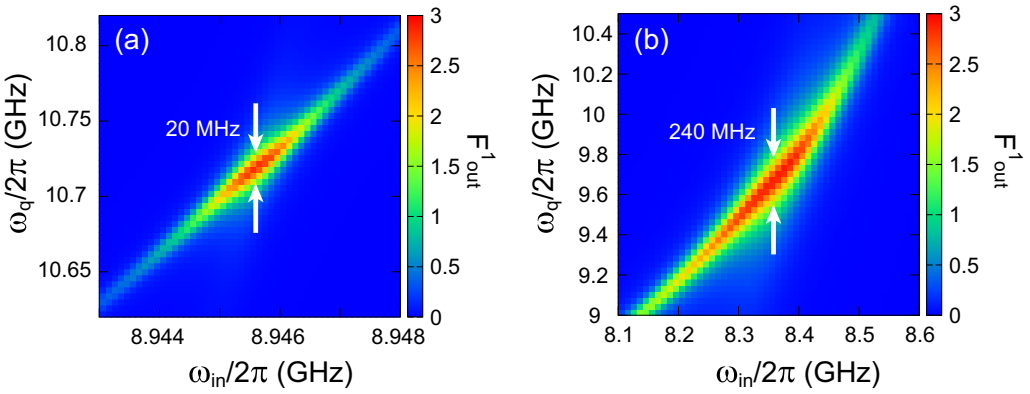

FIG. 5. Effect of qubit detuning. (a) Dependence of the down-converted flux $F^1_{\rm out}$ on ω_q and $\omega_{\rm in}$, for $g = 2\pi \times 0.3$ GHz and $\kappa_e = 2\pi \times 255$ kHz. $\kappa_i = \gamma = 0$ is assumed. (b) The same plot as (a) for $g = 2\pi \times 1.0$ GHz and $\kappa_e = 2\pi \times 35.4$ MHz.

drastically relaxed for $g = 2\pi \times 1.0$ GHz: $\kappa_i \lesssim 2\pi \times 12.7$ MHz ($Q_i \gtrsim 236$) and $\gamma \lesssim 2\pi \times 70.5$ MHz ($T_1 \gtrsim 2.26$ ns). We observe that the condition for the cavity is tighter than that for the qubit. This is because, in the present phenomenon, the qubit excited state is used only virtually to realize the effective coupling between $|g01\rangle$ and $|g30\rangle$ states. In Fig. 6(c), $F^1_{\rm out}$ is plotted as a function of $g_{\rm eff}$ and κ_i, employing the nearly optimal parameters ($\omega_q = \omega_q^{\rm opt}$, $\omega_{\rm in} = \omega_{\rm in}^{\rm opt}$, $\kappa_e = 1.25 g_{\rm eff}$) for each $g_{\rm eff}$. This figure serves as a phase diagram that visualizes the strong (weak) coupling regime to achieve efficient conversion, quantified by $g_{\rm eff} \gtrsim \kappa_i$ ($g_{\rm eff} \lesssim \kappa_i$). However, it is of note that this definition of strong/weak coupling regimes is slightly different from the usual one, since $g_{\rm eff} \sim \kappa_e$ in the present case.

D. Dependence on input photon rate

In the previous subsections, we discussed the down-conversion efficiency assuming a low input photon rate, in other words, the linear-response limit. Here, we observe the conversion efficiency for a higher input photon rate. In Fig. 7, we plot the dependence of the conversion efficiency on the input photon rate for various detuning of the input field. We observe that the efficiency decreases gradually for higher input photon rate. This is due to saturation of the atom-cavity system, which originates from the nonlinearity of the qubit. The star symbols in Fig. 7 represent the onset of saturation, which is given by

$$F_{\rm in} \sim \frac{(\kappa_e/2)^2 + (\Delta\omega)^2}{10\kappa_e}, \tag{30}$$

where $\Delta\omega$ is the detuning of the input field frequency from its optimal value. This is derived as follows. When one applies a monochromatic field $\mathcal{E}(t) = E_{\rm in} e^{-i\omega_{\rm in} t}$ to an empty one-sided cavity with an external decay rate κ_e, the mean intracavity photon number $\bar{n}$ is proportional to the drive photon rate $F_{\rm in} = |E_{\rm in}|^2$ and is given by $\bar{n} = \kappa_e F_{\rm in}/|\kappa_e/2 + i\Delta\omega|^2$. In the present system, the saturation effect due to nonlinearity would appear when the cavity is populated substantially. If we set this criterion at $\bar{n} \sim 0.1$ for example, the onset of saturation is estimated by Eq. (30). This explains the fact that the onset of saturation occurs at a higher input photon rate for a larger detuning.

VII. SUMMARY

We theoretically proved the possibility of the deterministic three-photon down-conversion of itinerant photons using a passive ultrastrong cavity-QED system, in which an atom is coupled to the first and third-harmonic cavity modes. For this

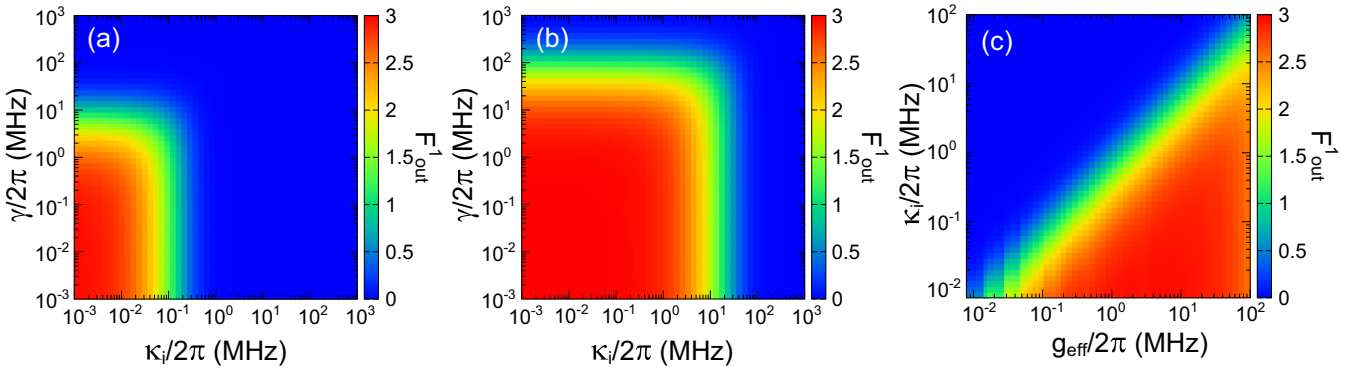

FIG. 6. Effect of intrinsic losses. (a) Dependence of the down-converted flux $F^1_{\rm out}$ on γ and κ_i, for $(g, \omega_q, \omega_{\rm in}) = 2\pi \times (0.3, 10.72, 8.9456)$ GHz and $\kappa_e = 2\pi \times 255$ kHz. (b) The same plot as (a), for $(g, \omega_q, \omega_{\rm in}) = 2\pi \times (1.0, 9.735, 8.378)$ GHz and $\kappa_e = 2\pi \times 35.4$ MHz. (c) Dependence of $F^1_{\rm out}$ on $g_{\rm eff}$ and κ_i. For each $g_{\rm eff}$, $\omega_q = \omega_q^{\rm opt}$, $\omega_{\rm in} = \omega_{\rm in}^{\rm opt}$, and $\kappa_e = 1.25 g_{\rm eff}$ are assumed.

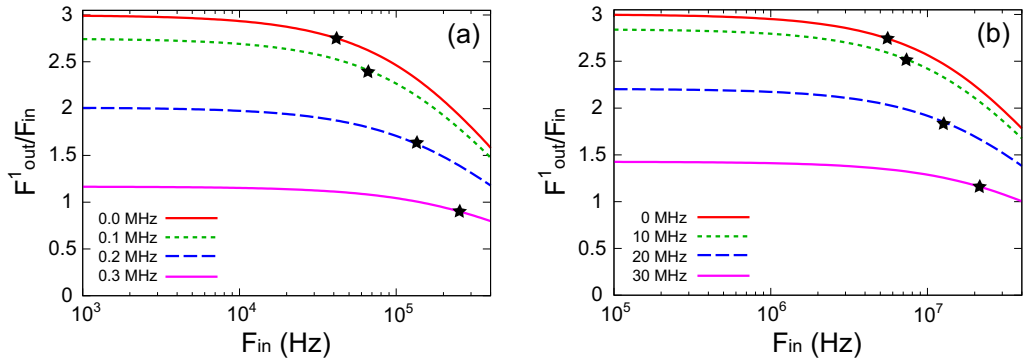

FIG. 7. Dependence of the down-conversion efficiency on the input photon rate, $F_{\rm in}$. Detuning of the input photon frequency from the optimal one, $(\omega_{\rm in} - \omega_{\rm in}^{\rm opt})/2\pi$, is indicated. Star symbols represent the onset of saturation [Eq. (30)]. (a) Results under the optimal condition in Fig. 4(a). (b) Results under the optimal condition in Fig. 4(b).

purpose, we developed an input-output formalism applicable to highly dissipative cavity-QED systems. The conditions for the deterministic conversion are as follows: (i) the frequencies of the qubit and the cavity modes are adequately chosen so that the two relevant levels ($|g30\rangle$ and $|g01\rangle$) are coupled effectively, and (ii) the cavity loss rates are adequately chosen so that they are comparable to the effective coupling. Such down-conversion is characteristic to the ultrastrong coupling regime of cavity QED, considering the upper limit of the intrinsic loss rates of the cavity.

ACKNOWLEDGMENTS

The author acknowledges fruitful discussions with I. Iakoupov, S. Goto, S. Ashhab, and F. Yoshihara. This work is supported in part by JST CREST (Grant No. JPMJCR1775) and JSPS KAKENHI (Grant No. 19K03684).

APPENDIX A: PERTURBATIVE EVALUATION OF $g_{\rm eff}$

In this Appendix, we analytically evaluate the effective coupling $g_{\rm eff}$ between $|g01\rangle$ and $|g30\rangle$ by the perturbative method called the generalized James' effective Hamiltonian method [49,50]. This method expand the Hamiltonian in series in the interaction picture so that the total Hamiltonian gives an accurate time evolution,

$$\hat{H}_{\rm eff}(t) = \sum_{n=2}^{\infty} \hat{H}_{\rm eff}^{(n)}(t),$$
$$\hat{H}_{\rm eff}^{(n)}(t) = i^{1-n} \int_0^t dt_1 \int_0^{t_1} dt_2 \cdots \int_0^{t_{n-2}} dt_{n-1} \times \hat{H}_I(t)\hat{H}_I(t_1)\cdots\hat{H}_I(t_{n-1}), \quad \text{(A1)}$$

where $\hat{H}_I(t)$ is the interaction part of the Hamiltonian in the interaction picture. In the qubit-cavity system considered here [see Eq. (1)], $\hat{H}_I(t)$ is given by

$$\hat{H}_I(t) = g_1(e^{-i\omega_q t}\hat{\sigma} + e^{i\omega_q t}\hat{\sigma}^\dagger)(e^{-i\omega_1 t}\hat{a}_1 + e^{i\omega_1 t}\hat{a}_1^\dagger) + g_3(e^{-i\omega_q t}\hat{\sigma} + e^{i\omega_q t}\hat{\sigma}^\dagger)(e^{-i\omega_3 t}\hat{a}_3 + e^{i\omega_3 t}\hat{a}_3^\dagger). \quad \text{(A2)}$$

The lowest-order interaction that couples $|g01\rangle$ and $|g30\rangle$ is of the 4th order, and the (time-dependent) effective coupling is given by $g_{\rm eff}(t) = \langle g01|\hat{H}_{\rm eff}^{(4)}(t)|g30\rangle$. By averaging out the oscillatory component [namely, $g_{\rm eff} = \lim_{T\to\infty} \frac{1}{T}\int_0^T dt\, g_{\rm eff}(t)$], the effective coupling is given by

$$g_{\rm eff} = \frac{\sqrt{6}g_1^3 g_3}{2\omega_1}\left(\frac{1}{(\omega_q - 3\omega_1)(\omega_q - \omega_1)} - \frac{1}{(\omega_q + 3\omega_1)(\omega_q + \omega_1)}\right). \quad \text{(A3)}$$

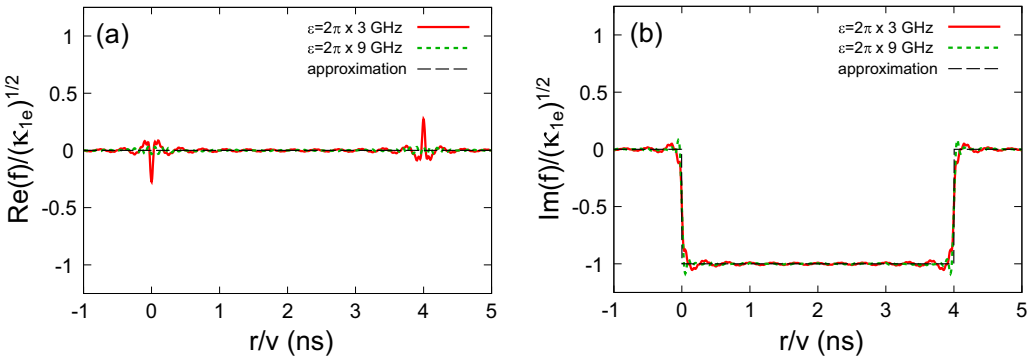

FIG. 8. Snapshots of f and $f_{\rm app}$ at $t = 4$ ns: (a) real and (b) imaginary parts. Solid (dotted) lines represent f for $\varepsilon = 2\pi \times 3$ GHz (9 GHz), and thin dashed lines represent $f_{\rm app}$. We assume a system-environment coupling of Eq. (28), and set the cutoff wavenumber at $k_x = 2\pi \times 20$ GHz.

For the weak-coupling case, ($g_1 = g_3 = 2\pi \times 0.3\,\mathrm{GHz}$ and $\omega_q = 2\pi \times 10.72\,\mathrm{GHz}$), g_{eff} amounts to 236.8 kHz from Eq. (A3), which roughly agrees with the numerically rigorous value of 222.5 kHz [Fig. 3(c)]. In contrast, for the strong-coupling case, ($g_1 = g_3 = 2\pi \times 1.0\,\mathrm{GHz}$ and $\omega_q = 2\pi \times 9.735\,\mathrm{GHz}$), g_{eff} amounts to 80.76 MHz from Eq. (A3), whereas the numerically rigorous value is 29.20 MHz. This discrepancy is due to the perturbative nature of Eq. (A3).

APPENDIX B: VALIDITY OF f_{app}

Here, we numerically compare f and f_{app} [Eqs. (16) and (17)] that appear when deriving the input-output relation. Their snapshots are shown in Fig. 8, assuming a concrete form [Eq. (28)] of the system-environment coupling. We confirm that f_{app} well approximates f for both the first- and third-harmonic cavity frequencies.

APPENDIX C: STATIONARY SOLUTION OF EQ. (21)

In this Appendix, we present the method to determine the stationary solution of Eq. (21) perturbatively. As the stationary solution, we employ the following form:

$$s_{ij}(t) = \sum_{p,q=0}^{\infty} \bar{s}_{ij}^{(p,q)} [\mathcal{E}_{\mathrm{in}}^*(t)]^p [\mathcal{E}_{\mathrm{in}}(t)]^q, \tag{C1}$$

where $\bar{s}_{ij}^{(p,q)}$ is time independent. Substituting Eq. (C1) into Eq. (21), we have

$$\sum_{m,n} \left(\eta_{ijmn}^{(1)} - i(p-q)\omega_{\mathrm{in}}\delta_{im}\delta_{jn}\right)\bar{s}_{mn}^{(p,q)} = -\sum_{m,n}\left(\eta_{ijmn}^{(2)}\bar{s}_{mn}^{(p-1,q)} + \eta_{ijmn}^{(3)}\bar{s}_{mn}^{(p,q-1)}\right), \tag{C2}$$

with the understanding that $\bar{s}_{ij}^{(p,q)} = 0$ if p or q is negative. This is a matrix equation, which determines $\bar{s}_{ij}^{(p,q)}$ from the lower-order quantities, $\bar{s}_{ij}^{(p-1,q)}$ and $\bar{s}_{ij}^{(p,q-1)}$. Note that this matrix equation is indeterminate for $p = q$. Then, we add the normalization condition of the density matrix,

$$\sum_{j=0}^{\infty} \bar{s}_{jj}^{(p,p)} = \delta_{p,0}. \tag{C3}$$

APPENDIX D: IMPEDANCE MATCHING CONDITION

We consider a linear system composed of two harmonic oscillators (oscillator 1 and 2) and two waveguides (waveguide 1 and 2), as depicted in Fig. 9. The two oscillators, which model the levels $|g01\rangle$ and $|g30\rangle$ of the main text, have the same resonance frequency ω_c and are coupled with a coupling constant g_{eff}. Oscillator j ($j = 1, 2$) is coupled to waveguide j with an external decay rate κ_j. We denote the annihilation operator of oscillator j by $\hat{a}_j$, and the input and output field-operators of waveguide j by $\hat{b}_{\mathrm{in},j}$ and $\hat{b}_{\mathrm{out},j}$, respectively. The Heisenberg equations for the two oscillators and the input-output relations are given by

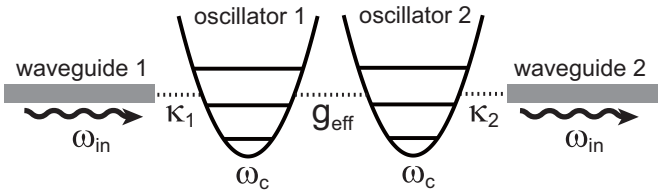

FIG. 9. Schematic of the coupled oscillators-waveguides system.

$$\frac{d}{dt}\hat{a}_1 = (-i\omega_c - \kappa_1/2)\hat{a}_1 - ig_{\mathrm{eff}}\hat{a}_2 - i\sqrt{\kappa_1}\hat{b}_{\mathrm{in},1}, \tag{D1}$$

$$\frac{d}{dt}\hat{a}_2 = (-i\omega_c - \kappa_2/2)\hat{a}_2 - ig_{\mathrm{eff}}\hat{a}_1 - i\sqrt{\kappa_2}\hat{b}_{\mathrm{in},2}, \tag{D2}$$

$$\hat{b}_{\mathrm{out},1} = \hat{b}_{\mathrm{in},1} - i\sqrt{\kappa_1}\hat{a}_1, \tag{D3}$$

$$\hat{b}_{\mathrm{out},2} = \hat{b}_{\mathrm{in},2} - i\sqrt{\kappa_2}\hat{a}_2. \tag{D4}$$

We apply a classical monochromatic field at frequency ω_{in} and amplitude E_{in} through waveguide 1, and apply no field through waveguide 2. Namely, $\langle\hat{b}_{\mathrm{in},1}\rangle = E_{\mathrm{in}}e^{-i\omega_{\mathrm{in}}t}$ and $\langle\hat{b}_{\mathrm{in},2}\rangle = 0$. Then, the equations of motion for the cavity and waveguide amplitudes are given by

$$\frac{d}{dt}\langle\hat{a}_1\rangle = (-i\omega_c - \kappa_1/2)\langle\hat{a}_1\rangle - ig_{\mathrm{eff}}\langle\hat{a}_2\rangle - i\sqrt{\kappa_1}\langle\hat{b}_{\mathrm{in},1}\rangle, \tag{D5}$$

$$\frac{d}{dt}\langle\hat{a}_2\rangle = (-i\omega_c - \kappa_2/2)\langle\hat{a}_2\rangle - ig_{\mathrm{eff}}\langle\hat{a}_1\rangle, \tag{D6}$$

$$\langle\hat{b}_{\mathrm{out},1}\rangle = \langle\hat{b}_{\mathrm{in},1}\rangle - i\sqrt{\kappa_1}\langle\hat{a}_1\rangle, \tag{D7}$$

$$\langle\hat{b}_{\mathrm{out},2}\rangle = -i\sqrt{\kappa_2}\langle\hat{a}_2\rangle. \tag{D8}$$

The stationary solution is readily obtained by the replacement of $d/dt \to -i\omega_{\mathrm{in}}$ in Eqs. (D5) and (D6). The transmission coefficient, $T = \langle\hat{b}_{\mathrm{out},2}\rangle/\langle\hat{b}_{\mathrm{in},1}\rangle$, is then given by

$$\frac{\langle\hat{b}_{\mathrm{out},2}\rangle}{\langle\hat{b}_{\mathrm{in},1}\rangle} = \frac{i\sqrt{\kappa_1\kappa_2}g_{\mathrm{eff}}}{\kappa_1\kappa_2/4 + g_{\mathrm{eff}}^2}. \tag{D9}$$

The impedance-matching condition, $|T| = 1$, reduces to $\sqrt{\kappa_1\kappa_2} = 2g_{\mathrm{eff}}$. This is in agreement with the optimal condition of the external cavity decay rate, $\kappa_e^{\mathrm{opt}} \sim g_{\mathrm{eff}}$, derived in Sec. VI A.

[1] E. M. Purcell, H. C. Torrey, and R. V. Pound, Resonance absorption by nuclear magnetic moments in a solid, Phys. Rev. **69**, 37 (1946).

[2] R. G. Hulet, E. S. Hilfer, and D. Kleppner, Inhibited Spontaneous Emission by a Rydberg Atom, Phys. Rev. Lett. **55**, 2137 (1985).

[3] W. Jhe, A. Anderson, E. A. Hinds, D. Meschede, L. Moi, and S. Haroche, Suppression of Spontaneous Decay at Optical Frequencies: Test of Vacuum-Field Anisotropy in Confined Space, Phys. Rev. Lett. **58**, 666 (1987).

[4] F. De Martini, G. Innocenti, G. R. Jacobovitz, and P. Mataloni, Anomalous Spontaneous Emission Time in a Microscopic Optical Cavity, Phys. Rev. Lett. **59**, 2955 (1987).

[5] S. Haroche and D. Kleppner, Cavity quantum electrodynamics, Phys. Today **42**(1), 24 (1989).

[6] M. Brune, F. Schmidt-Kaler, A. Maali, J. Dreyer, E. Hagley, J. M. Raimond, and S. Haroche, Quantum Rabi Oscillation: A Direct Test of Field Quantization in a Cavity, Phys. Rev. Lett. **76**, 1800 (1996).

[7] J. McKeever, A. Boca, A. D. Boozer, J. R. Buck, and H. J. Kimble, Experimental realization of a one-atom laser in the regime of strong coupling, Nature (London) **425**, 268 (2003).

[8] M. Keller, B. Lange, K. Hayasaka, W. Lange, and H. Walther, Deterministic coupling of single ions to an optical cavity, Appl. Phys. B **76**, 125 (2003).

[9] T. Yoshie, A. Scherer, J. Hendrickson, G. Khitrova, H. M. Gibbs, G. Rupper, C. Ell, O. B. Shchekin, and D. G. Deppe, Vacuum Rabi splitting with a single quantum dot in a photonic crystal nanocavity, Nature (London) **432**, 200 (2004).

[10] A. Wallraff, D. I. Schuster, A. Blais, L. Frunzio, R.-S. Huang, J. Majer, S. Kumar, S. M. Girvin, and R. J. Schoelkopf, Strong coupling of a single photon to a superconducting qubit using circuit quantum electrodynamics, Nature (London) **431**, 162 (2004).

[11] J. Johansson, S. Saito, T. Meno, H. Nakano, M. Ueda, K. Semba, and H. Takayanagi, Vacuum Rabi Oscillations in a Macroscopic Superconducting Qubit LC Oscillator System, Phys. Rev. Lett. **96**, 127006 (2006).

[12] A. A. Anappara, S. De Liberato, A. Tredicucci, C. Ciuti, G. Biasiol, L. Sorba, and F. Beltram, Signatures of the ultrastrong light-matter coupling regime, Phys. Rev. B **79**, 201303(R) (2009).

[13] T. Niemczyk, F. Deppe, H. Huebl, E. P. Menzel, F. Hocke, M. J. Schwarz, J. J. Garcia-Ripoll, D. Zueco, T. Hummer, E. Solano, A. Marx, and R. Gross, Circuit quantum electrodynamics in the ultrastrong-coupling regime, Nat. Phys. **6**, 772 (2010).

[14] T. Schwartz, J. A. Hutchison, C. Genet, and T. W. Ebbesen, Reversible Switching of Ultrastrong Light-Molecule Coupling, Phys. Rev. Lett. **106**, 196405 (2011).

[15] A. Bayer, M. Pozimski, S. Schambeck, D. Schuh, R. Huber, D. Bougeard, and C. Lange, Terahertz light-matter interaction beyond unity coupling strength, Nano Lett. **17**, 6340 (2017).

[16] F. Yoshihara, T. Fuse, S. Ashhab, K. Kakuyanagi, S. Saito, and K. Semba, Superconducting qubit-oscillator circuit beyond the ultrastrong-coupling regime, Nat. Phys. **13**, 44 (2017).

[17] A. F. Kockum, A. Miranowicz, S. De Liberato, S. Savasta, and F. Nori, Ultrastrong coupling between light and matter, Nat. Rev. Phys. **1**, 19 (2019).

[18] P. Forn-Diaz, L. Lamata, E. Rico, J. Kono, and E. Solano, Ultrastrong coupling regimes of light-matter interaction, Rev. Mod. Phys. **91**, 025005 (2019).

[19] E. Sanchez-Burillo, D. Zueco, J. J. Garcia-Ripoll, and L. Martin-Moreno, Scattering in the Ultrastrong Regime: Nonlinear Optics with One Photon, Phys. Rev. Lett. **113**, 263604 (2014).

[20] E. Sanchez-Burillo, J. J. Garcia-Ripoll, L. Martin-Moreno, and D. Zueco, Nonlinear quantum optics in the (ultra)strong light-matter coupling, Faraday Discuss. **178**, 335 (2015).

[21] A. F. Kockum, A. Miranowicz, V. Macri, S. Savasta, and F. Nori, Deterministic quantum nonlinear optics with single atoms and virtual photons, Phys. Rev. A **95**, 063849 (2017).

[22] R. Stassi, V. Macri, A. F. Kockum, O. Di Stefano, A. Miranowicz, S. Savasta, and F. Nori, Quantum nonlinear optics without photons, Phys. Rev. A **96**, 023818 (2017).

[23] A. F. Kockum, V. Macri, L. Garziano, S. Savasta, and F. Nori, Frequency conversion in ultrastrong cavity QED, Sci. Rep. **7**, 5313 (2017).

[24] M. Bock, A. Lenhard, C. Chunnilall, and C. Becher, Highly efficient heralded single-photon source for telecom wavelengths based on a PPLN waveguide, Opt. Express **24**, 23992 (2016).

[25] C. Couteau, Spontaneous parametric down-conversion, Contemp. Phys. **59**, 291 (2018).

[26] A. Anwar, C. Perumangatt, F. Steinlechner, T. Jennewein, and A. Ling, Entangled photon-pair sources based on three-wave mixing in bulk crystals, Rev. Sci. Instrum. **92**, 041101 (2021).

[27] Y. Yin, Y. Chen, D. Sank, P. J. J. O'Malley, T. C. White, R. Barends, J. Kelly, E. Lucero, M. Mariantoni, A. Megrant, C. Neill, A. Vainsencher, J. Wenner, A. N. Korotkov, A. N. Cleland, and J. M. Martinis, Catch and Release of Microwave Photon States, Phys. Rev. Lett. **110**, 107001 (2013).

[28] J. Wenner, Y. Yin, Y. Chen, R. Barends, B. Chiaro, E. Jeffrey, J. Kelly, A. Megrant, J. Y. Mutus, C. Neill, P. J. J. O'Malley, P. Roushan, D. Sank, A. Vainsencher, T. C. White, A. N. Korotkov, A. N. Cleland, and J. M. Martinis, Catching Time-Reversed Microwave Coherent State Photons with 99.4% Absorption Efficiency, Phys. Rev. Lett. **112**, 210501 (2014).

[29] K. Koshino, Down-conversion of a single photon with unit efficiency, Phys. Rev. A **79**, 013804 (2009).

[30] E. Sanchez-Burillo, L. Martin-Moreno, J. J. Garcia-Ripoll, and D. Zueco, Full two-photon down-conversion of a single photon, Phys. Rev. A **94**, 053814 (2016).

[31] K. Inomata, K. Koshino, Z. R. Lin, W. D. Oliver, J. S. Tsai, Y. Nakamura and T. Yamamoto, Microwave Down-Conversion with an Impedance-Matched Λ System in Driven Circuit QED, Phys. Rev. Lett. **113**, 063604 (2014).

[32] S.-P. Wang, G.-Q. Zhang, Y. Wang, Z. Chen, T. Li, J. S. Tsai, S.-Y. Zhu, and J. Q. You, Photon-dressed Bloch-Siegert Shift in an Ultrastrongly Coupled Circuit Quantum Electrodynamical System, Phys. Rev. Applied **13**, 054063 (2020).

[33] J. Douady and B. Boulanger, Experimental demonstration of a pure third-order optical parametric downconversion process, Opt. Lett. **29**, 2794 (2004).

[34] F. Gravier and B. Boulanger, Triple-photon generation: Comparison between theory and experiment, J. Opt. Soc. Am. B **25**, 98 (2008).

[35] M. Corona, K. Garay-Palmett, and A. B. U'Ren, Third-order spontaneous parametric down-conversion in thin optical fibers as a photon-triplet source, Phys. Rev. A **84**, 033823 (2011).

[36] N. A. Borshchevskaya, K. G. Katamadze, S. P. Kulik, and M. V. Fedorov, Three-photon generation by means of third-order spontaneous parametric down-conversion in bulk crystals, Laser Phys. Lett. **12**, 115404 (2015).

[37] K. Banaszek and P. L. Knight, Quantum interference in three-photon down-conversion, Phys. Rev. A **55**, 2368 (1997).

[38] C. W. S. Chang, C. Sabin, P. Forn-Diaz, F. Quijandria, A. M. Vadiraj, I. Nsanzineza, G. Johansson, and C. M. Wilson, Observation of Three-Photon Spontaneous Parametric Down-Conversion in a Superconducting Parametric Cavity, Phys. Rev. X **10**, 011011 (2020).

[39] H. Hubel, D. R. Hamel, A. Fedrizzi, S. Ramelow, K. J. Resch, and T. Jennewein, Direct generation of photon triplets using cascaded photon-pair sources, Nature (London) **466**, 601 (2010).

[40] D. R. Hamel, L. K. Shalm, H. Hubel, A. J. Miller, F. Marsili, V. B. Verma, R. P. Mirin, S. W. Nam, K. J. Resch, and T. Jennewein, Direct generation of three-photon polarization entanglement, Nat. Photonics **8**, 801 (2014).

[41] C. Ciuti and I. Carusotto, Input-output theory of cavities in the ultrastrong coupling regime: The case of time-independent cavity parameters, Phys. Rev. A **74**, 033811 (2006).

[42] A. Ridolfo, M. Leib, S. Savasta, and M. J. Hartmann, Photon Blockade in the Ultrastrong Coupling Regime, Phys. Rev. Lett. **109**, 193602 (2012).

[43] R. Stassi, S. Savasta, L. Garziano, B. Spagnolo, and F. Nori, Output field-quadrature measurements and squeezing in ultrastrong cavity-QED, New J. Phys. **18**, 123005 (2016).

[44] R. H. Lehmberg, Radiation from an N-Atom System. I. General Formalism, Phys. Rev. A **2**, 883 (1970).

[45] K. Koshino and Y. Nakamura, Control of the radiative level shift and linewidth of a superconducting artificial atom through a variable boundary condition, New J. Phys. **14**, 043005 (2012).

[46] K. Koshino, S. Kono, and Y. Nakamura, Protection of a Qubit via Subradiance: A Josephson Quantum Filter, Phys. Rev. Applied **13**, 014051 (2020).

[47] G. D. Mahan, *Many-Particle Physics*, 3rd edition (Springer, New York, 2000).

[48] Since the rigorous real-space representation is given by $\hat{c}_r = \widetilde{c}_r + \widetilde{c}_{-r}$ for $r > 0$, the commutation relation for $\widetilde{c}_r$ is given by $[\widetilde{c}_r + \widetilde{c}_{-r}, \widetilde{c}_{r'} + \widetilde{c}_{-r'}] = \delta(r - r')$ for $r, r' > 0$.

[49] D. F. V. James, Quantum computation with hot and cold ions: An assessment of proposed schemes, Fortschr. Phys. **48**, 823 (2000).

[50] W. Shao, C. Wu, and X. L. Feng, Generalized James' effective Hamiltonian method, Phys. Rev. A **95**, 032124 (2017).